Diamond & Related Materials 164 (2026) 113533

Contents lists available at ScienceDirect

Diamond & Related Materials

journal homepage: www.elsevier.com/locate/diamond

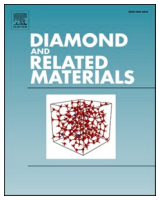

Modified laser-induced graphene as scaffold for the sensitive and selective sensing of pharmaceutical products

Sabrine Baachaoui [a,*], Ismaila Diedhiou [b], Sherif M.A.S. Keshk [c], Abdullah Y.A. Alzahrani [d], Noureddine Raouafi [e]

[a] Department of Chemistry, Faculty of Science, University of Tunis El Manar, Campus universitaire de Tunis El Manar, Tunis, 2092, Tunisia
[b] Laboratory of Organic Physical Chemistry and Environmental Analyses, Faculty of Science and Techniques, Cheikh Anta Diop University, Dakar, Fann, Senegal
[c] Become: Technology, Science, AI & Automation Lab., 63 rue de Tolbiac, Paris, 75013, France
[d] Department of Chemistry, Faculty of Science, King Khalid University, Abha, 61413, Saudi Arabia
[e] Basic and Applied Scientific Research Center (BASRC), Imam Abdulrahman Bin Faisal University, P.O. Box 1982, Dammam, 31441, Saudi Arabia

ARTICLE INFO

Keywords:
Graphitic carbon nitride
Graphene
Sensor
DLW
Modified electrode
Diclofenac

ABSTRACT

Diclofenac is a widely used pharmaceutical pollutant that is frequently detected in wastewater and natural waters; however, its reliable on-site quantification remains challenging because of costly instrumentation, labor-intensive sample preparation, and electrodes with limited electron-transfer efficiency. In this study, we report a simple, scalable, and mask-free strategy for constructing high-performance electrochemical electrodes based on laser-induced graphene (LIG) produced by direct laser graphene writing on polyimide. The porous three-dimensional LIG scaffold was subsequently functionalized with Co(II)-chelated graphitic carbon nitride (Co(II)@g-C_3N_4) to introduce redox-active sites and enhance interfacial charge transfer. Structural and electrochemical analyses revealed a seven-fold increase in the electrochemically active surface area and markedly improved heterogeneous electron-transfer kinetics after functionalization. Owing to these synergistic effects, the hybrid LIG electrodes enabled highly sensitive square-wave voltammetric detection of diclofenac over a wide linear range (1–200 μM), with a low detection limit of 0.10 μM (S/N = 3) and two distinct sensitivity regions. The sensor exhibited excellent selectivity toward diclofenac in the presence of common interferents and demonstrated reliable performance in pharmaceutical formulations and spiked human urine samples. This study highlights laser-induced graphene as a versatile and environmentally friendly electrode scaffold for advanced electrochemical sensing platforms in the pharmaceutical and environmental monitoring fields.

1. Introduction

Diclofenac, 2-(2-((2,6-dichlorophenyl)amino)phenyl)acetic acid, is a nonsteroidal anti-inflammatory drug that is widely used for its antipyretic and anti-inflammatory properties to alleviate pain and symptoms associated with arthritis. Despite its therapeutic benefits, diclofenac poses challenges in terms of biodegradation, and its removal in conventional wastewater treatment plants (WWTPs) is only partial, typically ranging from 20% to 40% [1]. Consequently, DF has been detected in effluents from WWTPs, surface water, groundwater, and drinking water at concentrations ranging from ng·L^{-1} to g·L^{-1} [2]. The widespread presence of diclofenac in aquatic bodies raises concerns owing to its persistence and potential long-term impact on both ecological systems and human health, even at low concentrations [3].

Conventional analytical methods are robust and accurate; however, they often require expensive equipment, involve lengthy analysis times, and require skilled technicians. Various conventional methods, such as high-performance liquid chromatography [4], gas chromatography [5], thin-layer chromatography [6], capillary zone electrophoresis [7], and spectrophotometry [8,9], have been used for DF determination. Although these methods are robust and accurate, they often require expensive equipment and involve lengthy analysis times. Recognizing the electroactivity of diclofenac, electrochemical approaches have gained attention as alternatives for its detection [10–13]. Electrochemical methods offer advantages such as high sensitivity, specificity, low detection limits, cost effectiveness, and simplicity. Furthermore, these methods are highly sensitive, specific, have low detection limits, are cost-effective, and are amenable. They comply well with the WHO

* Corresponding author.
E-mail addresses: sabrine.baachaoui@fst.utm.tn (S. Baachaoui), naraouafi@iau.edu.sa (N. Raouafi).

https://doi.org/10.1016/j.diamond.2026.113533
Received 14 January 2026; Received in revised form 1 March 2026; Accepted 10 March 2026
Available online 12 March 2026

ASSURED criteria for devising low-cost and easy-to-handle analytical methods for low-resource settings [14,15].

In direct electrochemical measurements of electroactive species, bare electrodes may exhibit low responsiveness. To address this, nanomaterials, mediators, and modified electrodes have been usd to enhance electrochemical response. Numerous research groups have developed electrochemical (bio)sensors for the rapid and sensitive detection of diclofenac in various samples and matrices [16]. These sensors typically consist of an electrode serving as a transduction element coated with a chemical recognition film to impart specific identification capabilities, resulting in highly selective sensors. However, there is a growing need to develop eco-friendly and cost-effective modified electrodes for the detection of diclofenac. Graphene-based sensors, which leverage the unique properties of graphene, have shown promise in applications spanning biology, medicine, and environmental monitoring [17–19]. Traditional methods of graphene production, such as mechanical exfoliation (ME), chemical vapor deposition (CVD), epitaxial growth (EG), and reduction of graphene oxide (rGO), have drawbacks: ME is inefficient, CVD and EG are energy-intensive and costly, and rGO contributes to environmental pollution during preparation [20,21]. Therefore, the development of a technique for graphene production that overcomes these limitations is of significant importance [22].

The laser direct-writing approach has gained significant attention in recent years owing to its advantages, including selective and localized reduction, accurate and rapid patterning, and the absence of masks and additional chemicals. In the context of graphene production, laser-induced graphene has been generated using two methods: reduction of graphene oxide (GO) and direct laser writing of graphene [23–25]. The former involves the photochemical/photophysical reduction of GO using laser irradiation with various types of lasers, resulting in LIG [26]. The latter involves the irradiation of polymer precursors, such as polyimide and phenolic resin, as well as natural materials, such as paper and wood, with a laser to produce LIG [23,24]. Doping has been used to enhance the range and sensitivity of laser-induced graphene (LIG)-based sensors. The formation of conductive channels between the dopants and LIG increases the number of microcracks and resistance, thereby improving the performance of stress and strain sensors. LIG has been applied in various sensors owing to its high sensitivity, wide detection range, rapid reaction time, and strong repeatability. For example, in stress sensors, LIG, which is mechanically durable, highly conductive, and sensitive to various stresses, exhibits altered capacitance and resistance, effectively translating force impulses into electrical signals [27]. Although the intrinsic electrical conductivity of laser-induced graphene ($\sim 10^2$–10^4 S·cm^{-1}) is lower than that of high-quality CVD graphene ($\sim 10^4$–10^5 S·cm^{-1}), it is comparable to or higher than that of most reduced graphene oxide films ($\sim 10^1$–10^3 S·cm^{-1}) [28,29], while offering key practical advantages such as direct mask-free fabrication, high accessible surface area, and abundant electrochemically active edge sites.

The success of electrochemical sensing depends on the electrode materials used, including metals, metal oxides, conducting polymers, and carbon nanostructures [30]. A portable electrode sensor based on laser-induced graphene has been reported for the electrochemical detection of carbendazim [29]. Several bioactive compounds, such as dopamine, uric acid, and paracetamol, have been detected at submicromolar levels using AuNP-modified LIG electrodes [31–33]. The addition of platinum nanoparticles to the surface of LIG improved the electrode sensitivity, demonstrating a large dynamic range varying from 1 to 40 μM, with a detection limit of 0.67 μM. In contrast, nickel nanoparticles and graphene oxide were synthesized and independently characterized using spectroscopic and microscopic methods [35]. The electrodeposition method was then used to create a novel glassy carbon electrode modified with electrochemically reduced graphene oxide coated with nickel nanoparticles for diclofenac detection. The sensing range of this platform was 0.25–125 μM. The limits of detection and quantification of the proposed method were determined to be 0.09 and 0.30 μM, respectively. Furthermore, a differential pulse voltammetric technique for determining DCF is presented, utilizing a glassy carbon electrode modified with zeolitic imidazolate framework-67/graphitic carbon nitride (ZIF-67/g-C_3N_4). The modified electrode exhibited acceptable repeatability, reproducibility, and selectivity toward DF in the range of 0.2–2.2 μmol·L^{-1} and had a detection limit of 0.071 μmol·L^{-1} [36]. For the first time, we offer a unique strategy for constructing conductive sensors for diclofenac by employing electrodes with sensitive detection limits, high surface areas, and laser scribing to generate graphene from a polyimide sheet. To boost the detection sensitivity, the LIG electrode surface was modified with Co(II)-functionalized graphitic carbon nitride (Co(II)@g-C_3N_4) nanoplates. To provide optimal performance, we optimized the LIG electrode production process and characterized the physicochemical parameters of the electrodes, including the heterogeneous electron transfer rate and electrochemically active surface area. Furthermore, by functionalizing the electrodes with gold nanoparticles, we improved the physicochemical characteristics of the electrodes, resulting in greater sensing capabilities for DCF and a reduced detection limit. Furthermore, we used a variety of analytical methods to gain insights into the structure, composition, and surface morphology of the (Co(II)@g-C_3N_4) films, including FTIR, X-ray diffraction (XRD), and SEM. This study demonstrates the enormous potential of LIG-based electrochemical sensors for a wide range of applications. We opened new opportunities in the industry by establishing a simple yet effective approach for producing highly conductive sensors and improving their characteristics through functionalization.

2. Methods

2.1. Apparatuses

SEM/EDAX measurements were performed using an F250 apparatus (Thermo Fisher). Raman spectra were recorded using a Horiba LabRAM HR800 system at 23 °C with a He—Ne laser (632.8 nm) at a power of 2.4 mW. X-ray diffraction was performed using a PANalytical XRD diffractometer with CuKα = 1.54 Å radiation measured at room temperature (RT).

Electrochemical measurements were performed using a Palmsens4 potentiostat equipped with an FRA module at RT. The experimental design and data were collected using PSTrace v5.10 software. The graphene electrodes were scribed on polyimide sheets using a 40 W laser machine equipped with a CO_2 laser source (λ = 10.6 μm).

2.2. Chemicals and reagents

All chemicals were purchased from Sigma-Aldrich (Germany) and used as received. Graphitic carbon nitride (g-C_3N_4) was prepared according to a previously reported method [37]. 1× PBS was prepared by dissolving NaCl, KCl, Na_2HPO_4, and KH_2PO_4 in deionized water. DI water, obtained by osmosis filtration using a Millipore system, was used for all preparations. Polyimide Kapton® scotch tape (thickness = 75 μm) was purchased from a local retailer for electronic components. A stock solution of diclofenac sodium salt was prepared by dissolving diclofenac sodium salt in PBS, and daughter solutions were prepared by dilution.

2.3. Preparation of Co(II)@g-C_3N_4

The g-C_3N_4 was synthesized via one-step pyrolysis of thiourea [37]. Specifically, 6.0 g of thiourea was calcined at 500 °C in a covered 50-mL ceramic crucible within a muffle furnace for 3 h, yielding a yellow powder. Subsequently, the powder was washed several times with ethanol to remove unreacted thiourea and dried overnight at 60 °C.

The Co(II)@g-C_3N_4 complex was synthesized by combining $CoCl_2$ with graphitic carbon nitride. Briefly, 1.0 mg of $CoCl_2$ was introduced into a 1.0 mg suspension of g-C_3N_4 in DI water (1.5 mL). The mixture

was sonicated at 42 Hz for 30 min, followed by centrifugation for 15 min at 10,000 rpm. The supernatant containing excess Co(II) was then removed. The solid was washed twice with DI water and redispersed in DI water prior to use.

2.4. Fabrication of the electrodes

A PI film with a thickness of 75–80 μm was first affixed to the surface of a polyethylene terephthalate film. A CAD three-electrode configuration was used to scribe the LIGEs using a water-cooled CO_2 laser scribing machine (Fig. 1). The laser power and speed were set to 6.0 W and 15.0 $cm{\cdot}s^{-1}$, respectively. These parameters were optimized in previous studies from our group [38,39]. The diameter of the working surface electrode was 0.5 cm, and the connectors were covered with a UV-curable polymer.

The Co(II)@g-C_3N_4-modified LIGEs were prepared by drop-casting 10 μL of the Co(II)@g-C_3N_4 suspension onto the surface of the working electrode. The drop was allowed to dry at room temperature. The electrode was then rinsed with DI water to remove non-adsorbed materials before use.

2.5. Electrochemistry

The bare and modified electrodes were fully characterized using cyclic voltammetry (CV) and electrochemical impedance spectroscopy (EIS). Electrochemical measurements were performed in 10 mM PBS, and the data were collected. The electrode surface was examined in a solution containing 5.0 mM ferrocenedimethanol, serving as the redox probe to evaluate the electrode kinetics and electrochemical surface area, and to determine the heterogeneous electron transfer rate. Square-wave voltammetry (SWV) was used to detect DF. The optimal operating parameters were a potential amplitude of 10 mV, potential step of 50 mV, and frequency of 25 Hz. Uric acid (UA), salicylic acid (SA), and ascorbic acid (AA) were examined as potential interfering molecules for selectivity.

2.6. Determining the heterogenous electron transfer rates

The Randles–Sevcik equation (Eq. 1) was used to estimate the electrochemically active surface areas of both bare LIGE and Co(II)@g-C_3N_4/LIGE [40].

$$i_p = \left(2.6 \times 10^{-5}\right) n^{3/2} A (Dv)^{1/2} C_0 \quad (1)$$

where i_p is expressed in amperes (A), A is the geometric area of the electrode in cm^2, C_0 is the concentration of the redox probe in $mol{\cdot}cm^{-3}$, n is the number of electrons participating in the redox reaction, v is the scan rate in $V{\cdot}s^{-1}$, and D is the diffusion coefficient in $cm^2{\cdot}s^{-1}$.

The Nicholson equation (Eq. 2) was used to determine the heterogeneous electron transfer (HET) rate (k^0) [41].

$$\psi = k^0 \left(\frac{D_0}{D_R}\right)^{\frac{\alpha}{2}} \bullet \left(\frac{RT}{\pi n F D_0 v}\right)^{\frac{1}{2}} \quad (2)$$

where ψ is the dimensionless kinetic parameter, k^0 is the HET rate, D_O and D_R are the diffusion coefficients of ferrocenedimethanol, α is the transfer coefficient, n is the number of electrons involved in the process ($n = 1$), F is the Faraday constant ($F = 96{,}489 C{\cdot}mol^{-1}$), v is the scan rate ($V{\cdot}s^{-1}$), and R is the gas constant (8.314 $J/mol{\cdot}K$), and T is the absolute temperature (K). This equation can be simplified if the values of D_O and D_R are approximately equal, as in this case, and α = 0.5 (Eqs. 3 and 4).

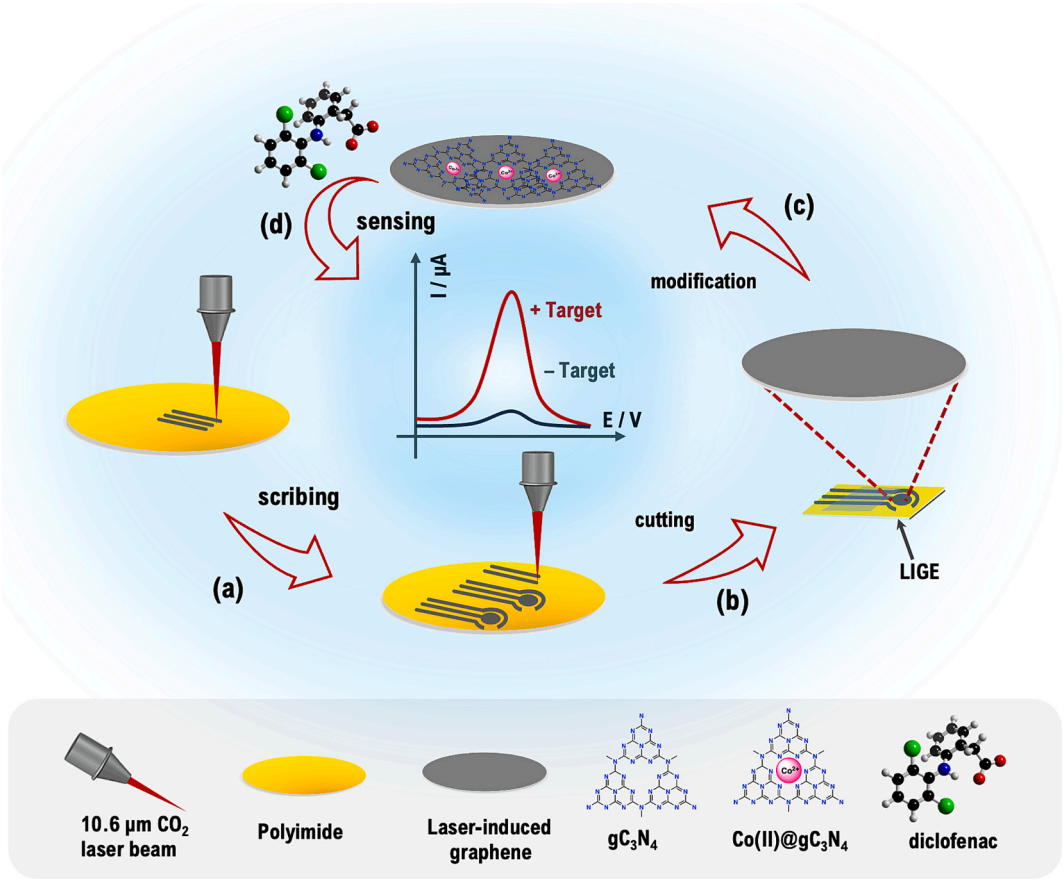

Fig. 1. Graphical illustration of the fabrication process of the modified laser-induced graphene electrodes: (a) direct laser writing, (b) cutting and insulating the electrodes with UV-curable polymers, (c) drop-casting of Co(II)@g-C_3N_4, and (d) sensing of diclofenac.

$$\psi = k^0 \left(\frac{RT}{\pi nFDv}\right)^{\frac{1}{2}} \quad (3)$$

Or simply,

$$\psi = k^0 \bullet \beta \bullet v^{-\frac{1}{2}}, \text{with } \beta = \left(\frac{RT}{\pi nFD}\right)^{\frac{1}{2}} \quad (4)$$

In this case, ψ depends only on ΔE_p and can be determined using Eq. 5.

$$\psi = \frac{-0.6288 + 0.0021X}{(1 - 0.017X)}, \text{Where } X = \Delta E < 300 \text{ mV} \quad (5)$$

The mass transport coefficient, m_T, was calculated using Eq. 6.

$$m_T = \sqrt{\frac{FDv}{RT}} \quad (6)$$

The Matsuda-Ayabe parameter for assessing the system reversibility was calculated using Eq. 7 [42].

$$\zeta = k^0 \bullet \left(\frac{RT}{FDv}\right)^{\frac{1}{2}} = \frac{k^0}{m_T} \quad (7)$$

From the complex impedance Z* (Eq. 8) and its real and imaginary (Z′ and Z″) components.

$$Z^*(\omega) = Z'(\omega) + jZ''(\omega) \quad (8)$$

The complex capacitance, derived from the complex impedance, is given by Eq. 9:

$$C^*(\omega) = C'(\omega) - jC''(\omega) \quad (9)$$

The real and imaginary capacitance components are derived from Z′ and Z″, respectively, according to Eqs. 10 and 11.

$$C'(\omega) = -\frac{Z''(\omega)}{\omega\left(Z'^2(\omega) + Z''^2(\omega)\right)} \quad (10)$$

$$C''(\omega) = \frac{Z'(\omega)}{\omega(Z'^2(\omega) + Z''^2(\omega))} \quad (11)$$

Finally, the in-plane crystallite size (L_a) was estimated using the Tuinstra–Koenig equation (Eq. 12) [43,44].

$$L_a(nm) = \frac{2.4 \times 10^{-10} \bullet \lambda^4}{I_D/I_G} \quad (12)$$

Where λ is the excitation laser wavelength and I_D/I_G is the ratio of the D to G bands of LIG.

3. Results

3.1. Preparation of the Co(II)@g-C_3N_4-modified LIGEs

The modified electrodes were prepared in two straightforward steps, starting with a commercial PI membrane affixed to a PET film to withstand high temperatures during the laser ablation process. Direct laser writing was used to prepare a series of computer-aided design electrodes with dimensions that matched those of commonly used screen-printed electrodes. The laser-induced conversion of polyimide into graphene occurs through synergistic photothermal and photochemical pathways driven by localized laser heating (local $T > 2500$ °C) and bond scission [45], yielding turbostratic, poorly ordered graphene domains with an in-plane crystallite size of approximately 124 nm. This choice was made to ensure the use of identical electrical connectors and small volumes of chemical reagents. In the next step, the electrodes were modified by drop casting small volumes of Co(II)@g-C_3N_4 onto the surface of bare LIGE. Nitrogen-chelated Co(II) complexes can be oxidized to Co(III) at relatively low potentials, resulting in a surface that is both more conductive and catalytic, which could enhance the efficient oxidation of DF.

3.2. Microscopic and spectroscopic characterizations

The electrodes were characterized using SEM, Raman spectroscopy, and XRD. Fig. 2a-b show the secondary electron SEM images of both unaltered and modified electrodes at various magnifications, illustrating a porous tunnel network on the electrode surface, which is a result of gas molecules during the laser ablation process. The SEM images of the modified electrode surfaces revealed flakes of graphitic carbon nitride. Furthermore, EDX chemical analysis of the surface showed that the materials formed contained carbon (93.8 wt%), oxygen (5.1 wt%), and a minor amount of nitrogen (1.1 wt%) resulting from the photochemical decomposition of the polyimide membranes. The EDX results for the modified electrode indicated an increase in the nitrogen content and the presence of cobalt at a low concentration (0.6 wt. %), stemming from the added Co(II)@g-C_3N_4.

Raman spectra were obtained for the electrode surface both prior and following the modification with Co(II)@g-C_3N_4 (Fig. 2c). The spectrum of unmodified polyimide displays several peaks located at 1150–1200 cm^{-1}, 1650 cm^{-1}, and between 2850 and 3100 cm^{-1}, which are attributed to the vibrational modes of the pristine polymer (Fig. S1). The unaltered electrode material exhibited distinctive graphene bands at ~1350 cm^{-1} (D band) linked to structural defects in laser-induced graphene, a second band at around 1560 cm^{-1} (G band) related to the carbon-carbon stretching, and the 2D harmonic band at ~2700 cm^{-1} [40]. Graphitic carbon nitride is characterized by the presence of four peaks at ~690, ~990, ~1360, and ~ 1560 cm^{-1} [46]. The first two peaks correspond to *s*-triazine vibrations, whereas the latter two are attributed to structural defects and the breathing of the 2D surface. The bands at ~1350 and ~ 1560 cm^{-1} overlapped with those of graphene, and the bands at approximately 690 and ~ 990 cm^{-1} were too weak to be detected owing to the low Co(II)@g-C_3N_4 content.

Using the modified Tuinstra–Koenig relation [44], the in-plane crystallite sizes were estimated to be 124 and 30 nm for pristine LIG and Co(II)@g-C_3N_4/LIG, respectively. However, because Co(II)@g-C_3N_4 was drop-casted over LIG, the Raman signal predominantly probes the outer modified surface, and the increase in the I_D/I_G ratio (from 0.31 to 1.28) may partially originate from overcoating rather than from intrinsic structural degradation of the underlying graphene lattice. Consequently, the estimated crystallite size of Co(II)@g-C_3N_4/LIG reflects the composite surface structure and should not be considered as a direct measure of the intrinsic graphene domain size.

The XRD patterns of both the pristine and modified graphene surfaces are shown in Fig. 2d. The presence of graphene is indicated by the characteristic large peaks corresponding to the (200) and (100) reflection planes, located at 25.8° and 54.0°, respectively. The XRD pattern of Co(II)@g-C_3N_4/LIG shows different patterns at ~16°, ~28°, and ~ 42° with graphitic carbon nitride. The broad (002) reflection indicates reduced stacking coherence and turbostratic disorder, which may include contributions from disordered carbon, wheras the calculated interlayer spacing ($d_{002} \approx 0.345$ nm) exceeds that of ideal graphite (0.335 nm), consistent with few-layer graphene with expanded interlayer spacing and structural defects.

3.3. Electrochemical characterizations

3.3.1. Fabrication reproducibility

First, we compared the electrochemical responses of five modified LIGEs prepared under the same conditions using cyclic voltammetry in a 10 mM phosphate-buffered saline solution containing 100 μM DF. This allowed us to assess the reproducibility of LIGEs. The data showed that the signal change from electrode to electrode was relatively low, proving that the electrode preparation method was satisfactory (Fig. S2).

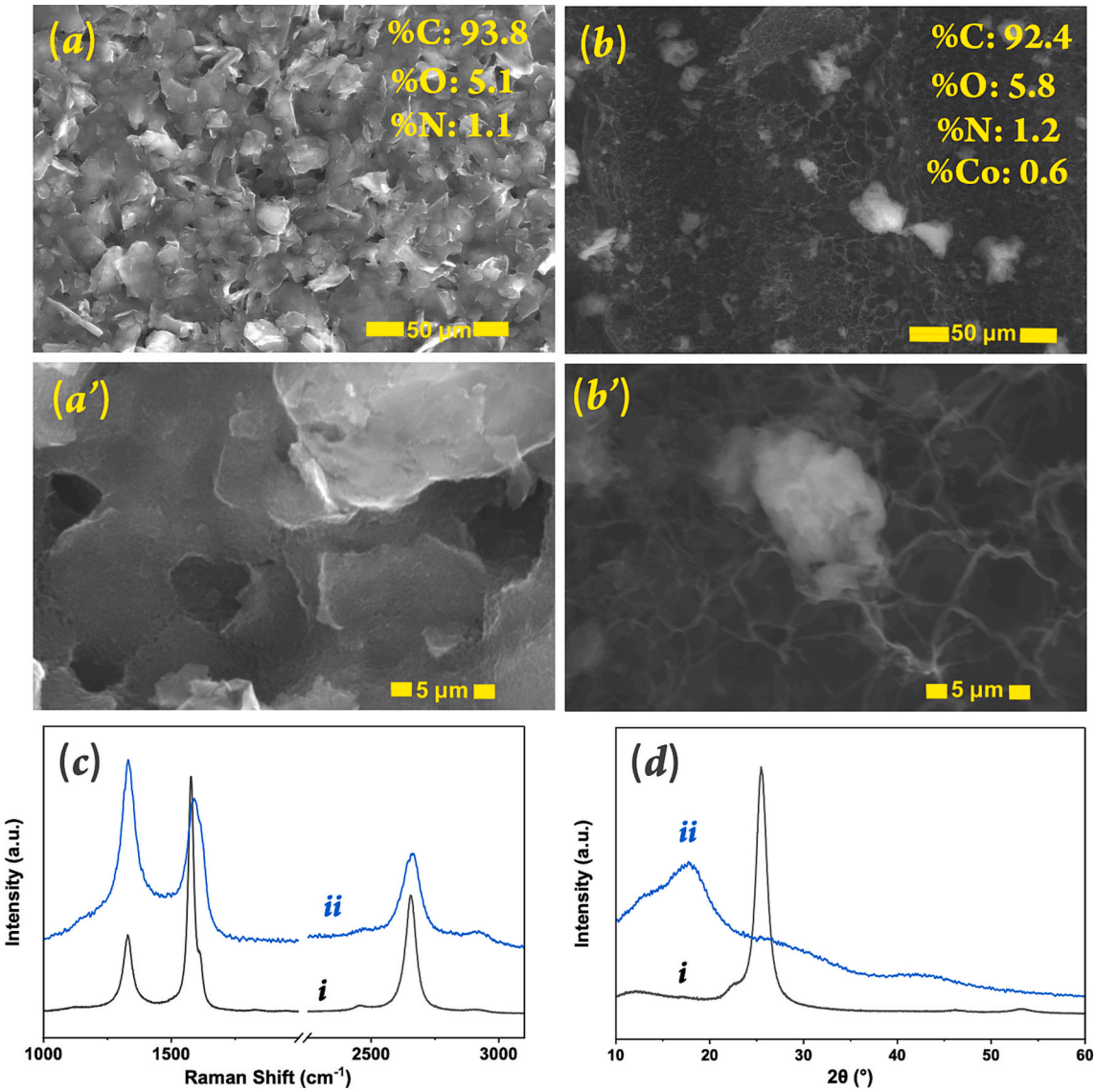

Fig. 2. Secondary electron SEM images at different magnifications (a-b) with the EDX composition analysis, Raman (c) and XRD (d) plots for the pristine (i) and modified (ii) electrode surfaces.

3.3.2. *Catalytic and enhancement effects*

The electrochemical activities of the bare LIGE, g-C_3N_4/LIGE, and Co(II)@g-C_3N_4/LIGE electrodes were evaluated in the presence of 100 µM DF dissolved in 10 mM PBS (Fig. 3a-b). The CV curves show higher current densities for the modified electrodes than those for the bare LIGE. The electroactivity of the electrodes varied in the following order: Co(II)@g-C_3N_4/LIGE > g-C_3N_4/LIGE > LIGE, implying the importance of modifying the LIGE electrode with Co(II)@g-C_3N_4. Furthermore, the data showed that the peak-to-peak potential differences were 254, 146, and 107 mV for LIGE, g-C_3N_4/LIGE, and Co(II)@g-C_3N_4/LIGE, respectively, suggesting the quasi-reversible behavior of these electrodes. Plotting the current density as a function of the square root of the scan rate showed a linear dependence, suggesting that the electrode kinetics were controlled by the diffusion of electroactive species (Fig. 3c-d). Notably, the area under the CV for the Co(II)@g-C_3N_4/LIGE electrode was significantly larger than that of the bare electrode, indicating that the Co(II)@g-C_3N_4/LIGE electrode can also be applied in faradaic capacitive sensing.

The addition of Co(II)@g-C_3N_4 to the LIGE surface induced a cathodic potential shift and improved the electron transfer kinetics, resulting in an increased redox current density. To understand this effect, the electrochemical activities of the modified and bare LIGEs were evaluated using water-soluble ferrocenedimethanol as the redox probe (Fig. 4). Hexacyanoferrate, hydroquinone, and catechol are commonly used as inner-sphere mediators to probe interfacial electron transfer mechanisms [32,33]. However, our data suggest that these probes are not applicable in this case because the peak-to-peak separation was greater than 300 mV, even at low scan rates, preventing their use in determining the heterogeneous electron transfer rate.

3.3.3. *Heterogeneous electron transfer rate*

The voltammograms in Fig. 4a and b show increased oxidation and reduction peak current densities with increasing scan rates for both electrodes, which is attributed to improved electrode kinetics. Furthermore, plotting the calibration curves of the redox current densities as a function of the square root of the scan rate (inset in Fig. 4a and b) revealed a linear dependence, suggesting diffusion-controlled kinetics, similar to those observed for diclofenac using the Co(II)@g-C_3N_4/LIG electrode.

Using (Eq. 5), the heterogeneous electron transfer rate, k^0, was determined from the slope of the plot of ψ as a function of the reciprocal of the scan rate (Fig. 4c). The k^0 values were $0.89 \pm 0.08 \times 10^{-3}$ and

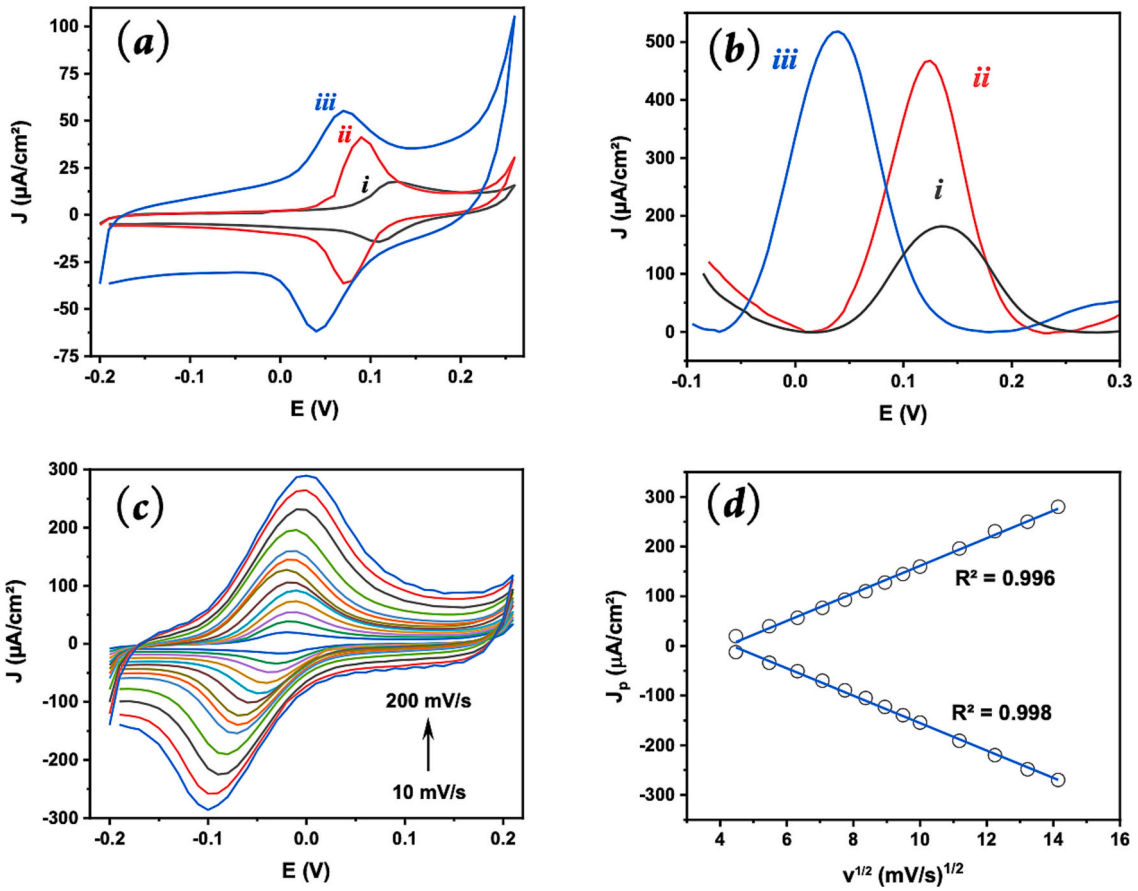

Fig. 3. CV (a) and SWV (b) plots for 100 μM diclofenac recorded using bare (*i*), g-C_3N_4 (*ii*), and Co(II)@g-C_3N_4-modified (*iii*) LIGEs recorded at 50 mV/s vs. Ag-Cl/Ag/KCl reference electrode. (c) CV plots recorded at different scan rates using Co(II)@g-C_3N_4-modified and (d) dependence of current density on the square root of scan rate.

$1.27 \pm 0.04 \times 10^{-3}$ cm·s^{-1} for the bare LIG and Co(II)@g-C_3N_4/LIG electrodes, respectively, representing an approximate increase of 43% after the modification. These values are roughly one order of magnitude lower than the values reported by Masood et al. (2.20×10^{-2} cm·s^{-1}) [47] for glassy carbon electrodes in a paracetamol solution with $LiClO_4$ as the supporting electrolyte, Griffiths et al. (2.37×10^{-2} cm·s^{-1}) for laser-induced GO reduction [48], and Silva et al. (5.2×10^{-3} cm s^{-1} and 4.5×10^{-3} cm s^{-1}) [49] using dopamine and acetaminophen as redox probes. Other studies using laser-induced graphene electrodes by Bosch-Navarro et al. (1.40×10^{-2} cm·s^{-1}) for CVD graphene [50] and Kavai et al. (3.20×10^{-2} cm·s^{-1}) [51] reported similar permeation rates. These differences are attributed to a slower electron transfer rate, as reflected by the larger peak separation (≈ 300 mV), which was higher than that observed in the aforementioned studies.

Furthermore, the mass transfer coefficient (Fig. S3A) increased linearly with the square root of the scan rate, consistent with diffusion-controlled transport, with a median value of 3.95×10^{-3} cm·s^{-1}. The Matsuda–Ayabe parameter plotted as a function of scan rate exhibited a pronounced decrease with increasing scan rate (Fig. S3B), with median values of 0.321 ± 0.028 and 0.446 ± 0.014 for the two electrodes, respectively. These values indicate quasi-reversible electron-transfer behavior ($\zeta < 15$) for both electrodes, with a ~ 39% improvement in the modified electrode compared to the pristine one.

3.3.4. Electrochemical surface area

Utilizing the Randles–Sevcik equation (Eq. 1), the electrochemically active areas for the various electrodes were determined to be 0.590, 0.824, and 1.392 cm^2, which are 3 to 7 times larger than the geometrical surface area (A_{geo} = 0.196 cm^2). This finding highlights the increased surface area attributable to the three-dimensional network in the laser-induced graphene and the advantageous effect of the deposited composite, which substantially augmented the three-dimensional surface area of the electrode.

3.3.5. Impedance and capacitance spectroscopies

Electrochemical impedance spectroscopy was performed to examine the other electrochemical characteristics of the electrodes. Fig. 4F shows Nyquist plots for both the modified and bare electrodes. A strong decrease in impedance was observed for the g-C_3N_4/LIG and Co(II)@g-C_3N_4/LIG electrodes, indicating an increase in the surface conductivity after adding g-C_3N_4 or Co(II)@g-C_3N_4. Furthermore, the Nyquist plots for the real and imaginary capacitance components showed an increase in capacitance in the following order: Co(II)@g-C_3N_4/LIGE > g-C_3N_4/LIGE > LIGE, confirming the increase in capacitance after modification of the LIGE electrode with the Co(II)@g-C_3N_4 composite. This was confirmed by the plots of the capacitance magnitudes of the three different electrodes.

3.4. Sensing of diclofenac

Square-wave voltammetry was used to detect diclofenac because it allows the removal of capacitive currents. The sensing performances of the bare and Co(II)@g-C_3N_4-modified electrodes were examined for comparison.

3.4.1. Using bare LIG electrode

First, a bare electrode was used in the presence of different DF concentrations. The peak current density increased with increasing DF

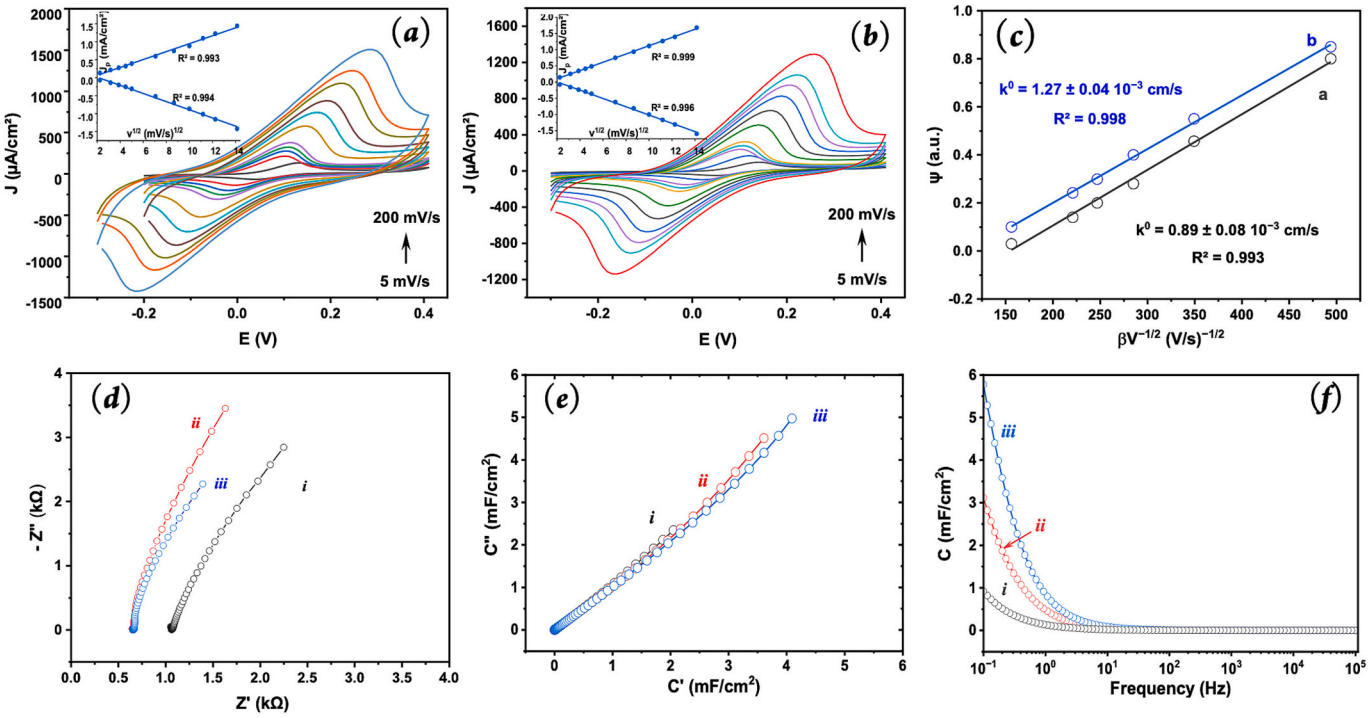

Fig. 4. CV curves recorded at different scan rates for the bare (a) and Co(II)@g-C_3N_4 (b) electrodes in a PBS solution containing 5 mM ferrocenedimethanol and corresponding plots of current densities versus scan rates (insets c and d). Plot of ψ versus the reciprocal of the scan rate to determine the heterogeneous electron transfer rate (e) and Nyquist plots of the three different electrodes (f) recorded in PBS.

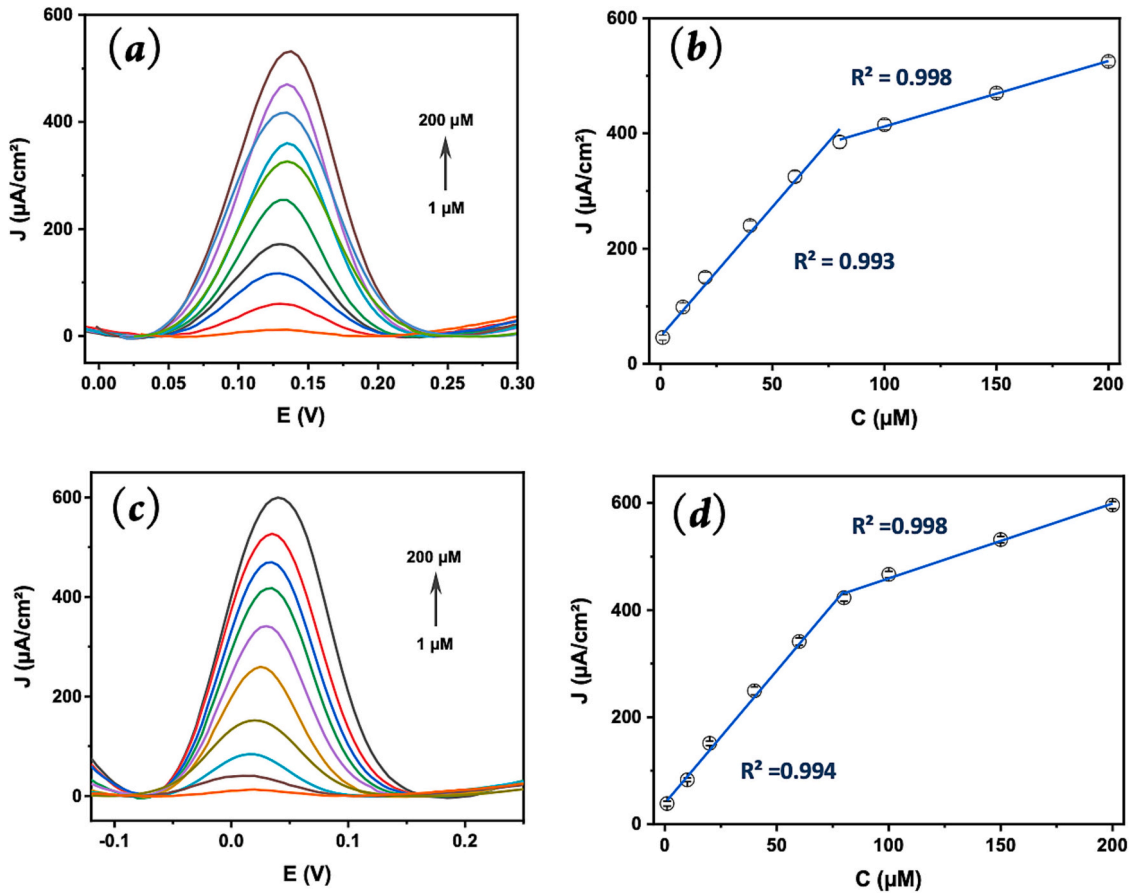

Fig. 5. (a and c) SWV plots and (b and d) corresponding calibration plots obtained with bare and Co(II)@g-C_3N_4 electrodes with increasing DF concentration.

concentration (Fig. 5a) at a relatively low oxidation potential of 0.13 V. The peak current density exhibited a linear dependence on DF concentration over two dynamic ranges of 1–80 μM and 80–200 μM, with Person's coefficients of 0.993 and 0.998, respectively (Fig. 5a). The sensitivities for the ranges were respectively 0.900 and 0.227 $\mu A \cdot \mu M^{-1} \cdot cm^{-2}$, denoting two different behaviors at low and high concentrations of the target analytes. The Eqs. (13) and (14) for the calibration curves are as follows:

$$j_p\ (\mu A \cdot cm^{-2}) = 0.90 \times [DF]\ (\mu M) + 9.84\ (R^2 = 0.993) \quad (13)$$

$$j_p\ (\mu A \cdot cm^{-2}) = 0.23 \times [DF]\ (\mu M) + 59.66\ (R^2 = 0.996) \quad (14)$$

The detection limit was calculated by dividing three times the standard deviation of the blank responses, σ_0 ($n = 10$), by the slope of the calibration curve, 0.4 μM.

3.4.2. Using Co(II)@g-C_3N_4-modified LIG electrode

Fig. 5c shows the increase in the peak current densities related to DF oxidation as a function of increasing concentration. The oxidation peak potential was 0.03 V, which is 0.1 V lower than that of the bare electrode, denoting the catalytic effect of the Co(II)@g-C_3N_4 complex. Plotting the current densities versus the DF concentration revealed a linear dependence (Fig. 5d). In this case, two dynamic ranges were observed: 1–80 and 80–200 μM, with correlation R-squared values of 0.994 and 0.998, respectively. The sensitivities were 10% and 23% higher than those of the bare electrode. Eqs. (15) and (16) are related to the calibration curves for these two ranges.

$$j_p\ (\mu A \cdot cm^{-2}) = 0.99 \times [DF]\ (\mu M) + 7.90\ (R^2 = 0,994) \quad (15)$$

$$j_p\ (\mu A \cdot cm^{-2}) = 0.28 \times [DF]\ (\mu M) + 63.89\ (R^2 = 0,998) \quad (16)$$

The detection limit for DF was 0.1 μM, which was four times lower than that of the bare electrode.

3.4.3. Selectivity

Using SWV at the same conditions, the simultaneous detection of DF, UA, and AA at a concentration of 100 μM for all three compounds was assayed. The plot shows three well-resolved and well-defined peaks at 0.03, 0.28, and 0.47 V for DF, UA, and AA, respectively. This result demonstrates the selectivity of the Co(II)g-C_3N_4 modified electrode, which can be used to analyze a mixture of drugs with interference (Fig. 6).

3.5. Detection of diclofenac in real samples

3.5.1. Commercial tablets

Solutions prepared by dissolving commercial DF tablets and doping urine samples with known amounts of DF were analyzed using the developed sensor. The results demonstrated a strong correlation between the added quantity and recovered concentration (Table 1). The recovery percentages ranged from 92.60 ± 8.37% to 102.33 ± 6.50%, indicating the high analytical performance of the prepared electrode.

3.5.2. Urine

A urine sample from a voluntary donor who had previously used diclofenac-containing medications was used to detect DF in a more complex sample. First, the sample was diluted five times with PBS and spiked with different DF concentrations. The recovery percentages ranged from 88.70 ± 15.55% to 96.45 ± 3.10%, indicating the high analytical performance of the prepared electrode.

3.6. Comparison with literature

Compared to other modified electrodes used for the detection of diclofenac, these electrodes presented very good performance in terms of a large dynamic range (1–200 μM) and a decent limit of detection of 0.3 μM (S/N = 3), without the need to modify the electrodes with noble metals (Au or Pt) [52,53], carbon nanotubes [10,54], or reduced graphene oxide [55] to improve their performance or extend their dynamic range. It is worth noting that DF concentrations below 1 μM were not assayed because the target drug concentrations in real samples are usually in the micromolar range. Using pulsed and anodic stripping

Table 1
Results for the analysis of spiked solutions of commercial diclofenac and urine samples.

Samples	$[DF]_{added}$ (μM)	$[DF]_{found}$ (μM)	%R* (±RSD) **
Tablet	20	19.30 ± 2.88	96.50 ± 14.40
	30	27.78 ± 2.51	92.60 ± 8.37
	40	38.85 ± 3.80	97.12 ± 9.50
	60	61.40 ± 3.90	102.33 ± 6.50
	100	94.77 ± 2.77	94.77 ± 2.77
Urine	20	17.74 ± 3.11	88.70 ± 15.55
	40	38.06 ± 2.80	95.15 ± 7.00
	60	55.73 ± 3.42	92.88 ± 5.70
	80	72.73 ± 3.78	90.91 ± 4.72
	100	96.45 ± 3.10	96.45 ± 3.10

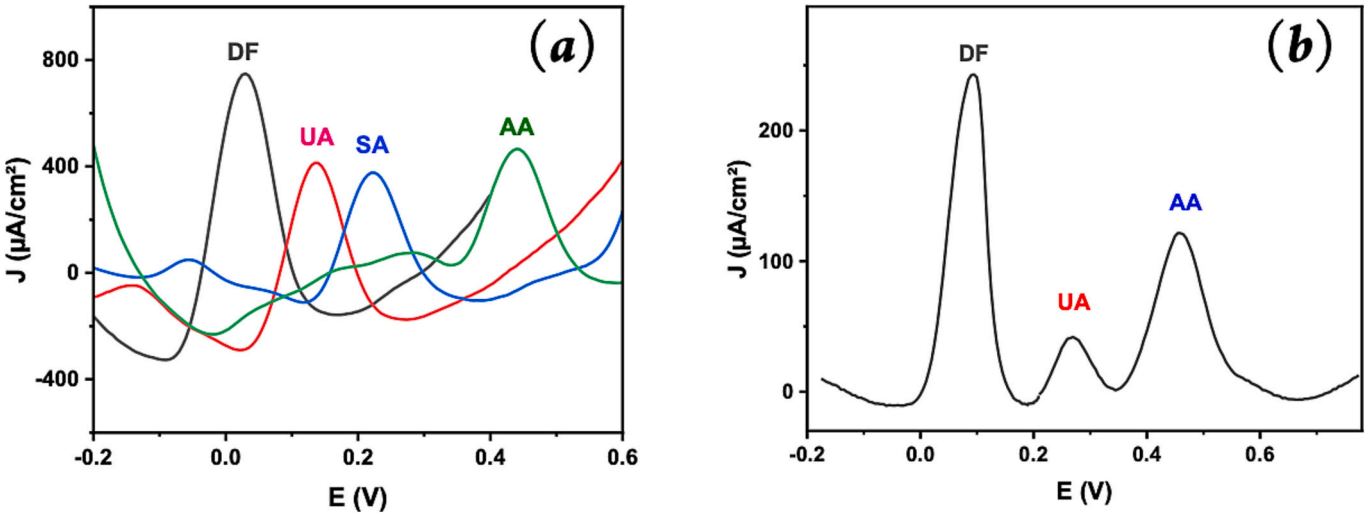

Fig. 6. (a) Individual SWV curves for DF, UA, SA, and AA, and (b) simultaneous DF, UA, and AA recorded using the Co(II)@g-C_3N_4/LIG electrode.

techniques, such as DPV, SWV, and SWASV, this electrode and others showed that they can be used to determine diclofenac in real samples, such as human serum [10], pharmaceutical tablets [10,53,56], and human or synthetic urine samples [52,55,57]. To the best of our knowledge, this is the first example of a sensor based on laser-induced graphene for diclofenac detection (Table 2).

4. Discussion

This study demonstrates the successful fabrication and functionalization of a few layers of turbostratic laser-induced graphene electrodes using a simple, rapid, and eco-friendly direct laser writing technique, followed by surface modification with Co(II)-chelated graphitic carbon nitride. Raman data analysis showed that the in-plane crystallite sizes were 124 and 30 nm for the bare and Co(II)@g-C_3N_4/LIGE, respectively. The combination of porous 3D laser-induced graphene and the catalytic/electron-mediating properties of Co(II)@g-C_3N_4 led to significant improvements in the physicochemical and electrochemical performances of the electrodes. Moreover, the cost of electrode production is minimal, and the electrodes are designed for single-use, which is essential for bioanalytical purposes [58]. The estimated material cost is less US$ 0.01 per electrode.

Microscopic and spectroscopic analyses confirmed the formation of a high-surface-area porous LIG structure decorated with uniformly distributed Co(II)@g-C_3N_4 nanosheets. The increased weight percentages of nitrogen and cobalt on the surface, along with the observed shifts in the Raman and XRD profiles, validated the successful modification. These structural changes directly translated into superior electrochemical performance. Cyclic voltammetry showed a clear enhancement in the current density and reduced peak-to-peak separation after modification, indicating accelerated electron transfer. The heterogeneous electron transfer rate increased by approximately 43%, and the electroactive surface area became seven times larger than the geometric area, strongly suggesting that the Co(II)@g-C_3N_4 coating increased the abundance of catalytic sites and improved the electronic conductivity. Furthermore, the calculated mass transport coefficients and Matsuda–Ayabe parameters increased by 39% supported these findings, respectively.

Table 2
Key performances of sensors for diclofenac.

Electrode	Detection technique	Dynamic range (μM)	Detection limit (μM)	Real sample	Ref.
PtNfs/rGO/SPCE	DPV	0.1–100	0.04	Urine	[52]
AuNPs/MWCNTs/GCE	DPV	0.03–200	0.02	Urine/Tablets	[53]
fCNTs/ZnO/GCE	SWASV		78 10^{-9}		[54]
MWCNT-$BMIMPF_6$/CCE	DPV	0.05–50	0.018	Serum/Tablets	[10]
ZnO/rGO/GCE	i-t	0.05–36.5	0.018	Urine	[55]
$Co(OH)_2$-rGO/CPE	SWASV	0.025–1.55	0.008	Urine/Tablets	[56]
CD-N/MoO_3NPs/SPCE	DPV	0.25–50	0.08	Urine	[57]
Bare LIGE	SWV	1–200	0.3	Not tested	This work
Co(II)@g-C_3N_4/LIGE	SWV	1–200	0.3	Urine/Tablets	This work

AuNPs: gold nanoparticles; CD-N: nitrogen-doped biomass carbon; CPE: carbon paste electrode; $BMIMPF_6$:1,4-butylmethylimidazolium,PF_6; DPV: differential pulse voltammetry; fCNTs: functionalized carbon nanotubes; GCE: glassy carbon electrodes; MWCNTs: multiwalled carbon nanotubes; rGO: reduced graphene oxide; SWASV: square wave anodic stripping voltammetry.

Electrochemical impedance spectroscopy further supported this enhancement: both the charge-transfer resistance and overall impedance decreased substantially, whereas the capacitance increased in the order LIGE < g-C_3N_4/LIGE < Co(II)@g-C_3N_4/LIGE. These findings reflect faster charge transport and superior interfacial properties, which are consistent with the kinetic parameters of the electrodes. These are essential for the sensitive detection of electroactive molecules.

Diclofenac, an environmentally persistent and clinically relevant pharmaceutical, was selected as the model analyte to assess sensor performance. Both the bare and modified electrodes exhibited two distinct linear response ranges (1–80 and 80–200 μM); however, Co(II)@g-C_3N_4/LIGE clearly outperformed unmodified LIGE. The modified electrode provided higher sensitivities (10% and 23% improvements), a lower oxidation potential (shift of ~100 mV), and a fourfold lower detection limit (0.10 μM vs. 0.40 μM for bare LIGE). These enhancements stem from the synergistic effect between the conductive graphene network and redox-active Co(II)/Co(III) centers within g-C_3N_4, which facilitates the oxidation of diclofenac.

In addition to sensitivity, the modified electrode demonstrated excellent selectivity toward DF, even in the presence of common interfering species, such as uric acid, ascorbic acid, and salicylic acid. The ability to resolve these analytes through well-separated oxidation peaks highlights the suitability of the electrode for complex matrices. High recovery values (88.7–102.3%) obtained from commercial tablet solutions and spiked urine samples further confirmed the analytical reliability and practical applicability of the sensor.

Compared with previously reported DF sensors, including those based on nickel nanoparticles, metal–organic frameworks, or noble metals, Co(II)@g-C_3N_4/LIGE offers a competitive or superior detection range, low detection limit, excellent selectivity, and a fabrication method that is both low-cost and environmentally friendly. This positions the proposed platform as a promising alternative to more resource-intensive methods of graphene production and electrode modification.

In summary, the findings highlight that combining direct laser writing with rational surface functionalization provides an effective strategy for producing high-performance electrochemical sensors. The versatility of LIG fabrication and tunability of g-C_3N_4-based modifiers offer opportunities to extend this approach to a broad range of pharmaceutical, biological, and environmental analytes.

5. Conclusion

This work suggests a straightforward and scalable technique for fabricating high-performance electrochemical sensors. It incorporates direct laser writing of polyimide with Co(II)-chelated graphitic carbon nitride surface modification. The Co(II)@g-C_3N_4 hybrid electrode addresses the limitations of conventional diclofenac detection technologies, including sluggish electron transfer kinetics, limited active surface area, and costly fabrication techniques. The incorporation of a porous 3D laser-induced graphene network and redox-active Co(II)/Co(III) sites increased the electron transfer rate and electrochemically active surface area, allowing for sensitive square-wave voltametric detection of diclofenac over a wide linear range (1–200 μM) with a LOD of 0.10 μM. The electrode also showed high selectivity against common interferents and consistent performance in pharmaceutical tablets and spiked urine samples, proving its durability in complex matrices. This study demonstrates that Co(II)-chelated g-C_3N_4/LIGE is a cost-effective, mask-free, and environmentally friendly sensing platform with significant potential for real-world pharmacological monitoring and environmental studies.

CRediT authorship contribution statement

Sabrine Baachaoui: Writing – original draft, Investigation, Formal analysis, Data curation. **Ismaila Diedhiou:** Writing – original draft, Software, Formal analysis. **Sherif M.A.S. Keshk:** Writing – review & editing, Resources. **Abdullah Y.A. Alzahrani:** Writing – review &

editing, Funding acquisition. **Noureddine Raouafi:** Writing – review & editing, Project administration, Investigation, Conceptualization.

Declaration of competing interest

The authors declare that they have no known competing financial interests or personal relationships that could have appeared to influence the work reported in this paper.

Appendix A. Supplementary data

Raman spectra of the polyimide and laser-induced graphene (Fig. S1), normalized current response for different electrodes ($n = 5$) prepared by dropcasting of Co(II)@g-C_3N_4 in the absence and presence of 100 μM of diclofenac (Fig. S2), plots of the mass transport coefficient and Matsuba-Ayabe parameters as a function of the scan rate for the various electrodes (Fig. S3) and the median values of the mass transport coefficients and the calculated Matsuba–Ayabe parameters as a function of the scan rate (Table S1) that supports the data presented in the main manuscript. Supplementary data to this article can be found online at [https://doi.org/10.1016/j.diamond.2026.113533].

Data availability

Data will be made available on request.

References

[1] H. He, J. Zhao, The efficient degradation of diclofenac by ferrate and peroxymonosulfate: performances, mechanisms, and toxicity assessment, Environ. Sci. Pollut. Res. Int. 30 (2023) 11959–11977, https://doi.org/10.1007/s11356-022-22967-0.

[2] M. Huguet, M. Deborde, S. Papot, H. Gallard, Oxidative decarboxylation of diclofenac by manganese oxide bed filter, Water Res. 47 (2013) 5400–5408, https://doi.org/10.1016/j.watres.2013.06.016.

[3] W. Zhao, Z. Duan, Z. Zheng, B. Li, Cobalt bismuth oxide with cobalt(II/III) as a new stable peroxymonosulfate activator for effective degradation, mineralization, and detoxification of diclofenac in water, J. Clean. Prod. 365 (2022) 132781, https://doi.org/10.1016/j.jclepro.2022.132781.

[4] S. Labhade, S. Chaudhari, R. Saudagar, Development and validation of RP-HPLC method for simultaneous determination of diclofenac sodium and tizanidine hydrochloride in bulk and tablet formulation, J. Analyt. Pharma. Res. 7 (2018), https://doi.org/10.15406/japlr.2018.07.00233.

[5] G. Dowling, P. Gallo, S. Fabbrocino, L. Serpe, L. Regan, Determination of ibuprofen, ketoprofen, diclofenac and phenylbutazone in bovine milk by gas chromatography-tandem mass spectrometry, Food Addit. Contam. Part A Chem. Anal. Control Expo. Risk Assess. 25 (2008) 1497–1508, https://doi.org/10.1080/02652030802383160.

[6] R. Bhushan, D. Gupta, A. Mukherjee, Liquid chromatographic analysis of certain commercial formulations for non-opioid analgesics, Biomed. Chromatogr. 21 (2007) 1284–1290, https://doi.org/10.1002/bmc.885.

[7] W. Jin, J. Zhang, Determination of diclofenac sodium by capillary zone electrophoresis with electrochemical detection, J. Chromatogr. A 868 (2000) 101–107, https://doi.org/10.1016/S0021-9673(99)01149-8.

[8] L.A. Carreira, M. Rizk, Y. El-Shabrawy, N.A. Zakhari, S.S. Toubar, Europium(III) ion probe spectrofluorometric determination of diclofenac sodium, J. Pharm. Biomed. Anal. 13 (1995) 1331–1337, https://doi.org/10.1016/0731-7085(95)01567-5.

[9] R.L. de Souza, M. Tubino, Spectrophotometric determination of diclofenac in pharmaceutical preparations, J. Braz. Chem. Soc. 16 (2005) 1068–1073, https://doi.org/10.1590/S0103-50532005000600026.

[10] K. Sarhangzadeh, A.A. Khatami, M. Jabbari, S. Bahari, Simultaneous determination of diclofenac and indomethacin using a sensitive electrochemical sensor based on multiwalled carbon nanotube and ionic liquid nanocomposite, J. Appl. Electrochem. 43 (2013) 1217–1224, https://doi.org/10.1007/s10800-013-0609-3.

[11] A.-R. Măghinici, A.-V. Bounegru, C. Apetrei, Electrochemical detection of diclofenac using a screen-printed electrode modified with graphene oxide and Phenanthroline, Chemosensors 13 (2025), https://doi.org/10.3390/chemosensors13020055.

[12] W. Boumya, N. Taoufik, M. Achak, H. Bessbousse, A. Elhalil, N. Barka, Electrochemical sensors and biosensors for the determination of diclofenac in pharmaceutical, biological and water samples, Talanta Open 3 (2021) 100026, https://doi.org/10.1016/j.talo.2020.100026.

[13] L. Tang, Y. Huang, Y. Wang, H. Zhao, A flexible electrochemical sensor for simultaneous detection of acetaminophen and diclofenac sodium using a carbon nanotube-doped hydrogel, J. Electron. Mater. 54 (2025) 6218–6228, https://doi.org/10.1007/s11664-025-12056-6.

[14] S. Smith, J.G. Korvink, D. Mager, K. Land, The potential of paper-based diagnostics to meet the ASSURED criteria, RSC Adv. 8 (2018) 34012–34034, https://doi.org/10.1039/C8RA06132G.

[15] R.W. Peeling, K.K. Holmes, D. Mabey, A. Ronald, Rapid tests for sexually transmitted infections (STIs): the way forward, Sex. Transm. Infect. 82 (2006) v1–v6, https://doi.org/10.1136/sti.2006.024265.

[16] W. Boumya, N. Taoufik, M. Achak, N. Barka, Chemically modified carbon-based electrodes for the determination of paracetamol in drugs and biological samples, J. Pharma. Analys. 11 (2021) 138–154, https://doi.org/10.1016/j.jpha.2020.11.003.

[17] A. Rabti, N. Raouafi, A. Merkoci, Bio(sensing) devices based on ferrocene-functionalized graphene and carbon nanotubes, CARBON 108 (2016) 481–514, https://doi.org/10.1016/j.carbon.2016.07.043.

[18] A. Rabti, C.C. Mayorga-Martinez, L. Baptista-Pires, N. Raouafi, A. Merkoçi, Ferrocene-functionalized graphene electrode for biosensing applications, Anal. Chim. Acta 926 (2016) 28–35.

[19] M. Zouari, S. Campuzano, J.M. Pingarrón, N. Raouafi, Femtomolar direct voltammetric determination of circulating miRNAs in sera of cancer patients using an enzymeless biosensor, Anal. Chim. Acta 1104 (2020) 188–198.

[20] Z. Yang, S. Xu, L. Zhao, J. Zhang, Z. Wang, X. Chen, X. Cheng, F. Yu, X. Zhao, A new direct growth method of graphene on Si-face of 6H-SiC by synergy of the inner and external carbon sources, Appl. Surf. Sci. 436 (2018) 511–518, https://doi.org/10.1016/j.apsusc.2017.11.252.

[21] K. Yi, D. Liu, X. Chen, J. Yang, D. Wei, Y. Liu, D. Wei, Plasma-enhanced chemical vapor deposition of two-dimensional materials for applications, Acc. Chem. Res. 54 (2021) 1011–1022, https://doi.org/10.1021/acs.accounts.0c00757.

[22] S. Perumal, R. Atchudan, I.W. Cheong, Recent studies on dispersion of graphene–polymer composites, Polymers 13 (2021) 2375, https://doi.org/10.3390/polym13142375.

[23] Z. Wan, E.W. Streed, M. Lobino, S. Wang, R.T. Sang, I.S. Cole, D.V. Thiel, Q. Li, Laser-reduced graphene: synthesis, properties, and applications, Adv. Mater. Technol. 3 (2018) 1700315, https://doi.org/10.1002/admt.201700315.

[24] J. Lin, Z. Peng, Y. Liu, F. Ruiz-Zepeda, R. Ye, E.L.G. Samuel, M.J. Yacaman, B. I. Yakobson, J.M. Tour, Laser-induced porous graphene films from commercial polymers, Nat. Commun. 5 (2014) 5714, https://doi.org/10.1038/ncomms6714.

[25] Z. Wan, X. Chen, M. Gu, Institute of Photonic Chips, University of Shanghai for Science and Technology, Shanghai 200093, China, Centre for Artificial-Intelligence Nanophotonics, School of Optical-Electrical and Computer Engineering, University of Shanghai for Science and Technology, Shanghai 200093, China, Laser scribed graphene for supercapacitors, OEA 4 (2021) 200079, https://doi.org/10.29026/oea.2021.200079.

[26] T.X. Tran, H. Choi, C.H. Che, J.H. Sul, I.G. Kim, S.-M. Lee, J.-H. Kim, J.B. In, Laser-induced reduction of graphene oxide by intensity-modulated line beam for supercapacitor applications, ACS Appl. Mater. Interfaces 10 (2018) 39777–39784, https://doi.org/10.1021/acsami.8b14678.

[27] Y. Zhu, J. Li, H. Cai, Y. Wu, H. Ding, N. Pan, X. Wang, Highly sensitive and skin-like pressure sensor based on asymmetric double-layered structures of reduced graphite oxide, Sens. Actuators B 255 (2018) 1262–1267, https://doi.org/10.1016/j.snb.2017.08.116.

[28] P. Chen, et al., Enhancing the conductivity of laser-induced graphene via a facile high-crystallinity-riveting method for multifunctional applications, ACS Appl. Mater. Interfaces 17 (2025) 64771–64782, https://doi.org/10.1021/acsami.5c18748.

[29] H.J. Sim, Z. Li, P. Xiao, H. Lu, The influence of lateral size and oxidation of graphene oxide on its chemical reduction and electrical conductivity of reduced graphene oxide, Molecules 27 (2022) 7840, https://doi.org/10.3390/molecules27227840.

[30] A.M. Campos, P.A. Raymundo-Pereira, C.D. Mendonça, M.L. Calegaro, S.A. S. Machado, O.N. Oliveira Jr., Size control of carbon spherical shells for sensitive detection of paracetamol in sweat, saliva, and urine, ACS Appl. Nano Mater. 1 (2018) 654–661, https://doi.org/10.1021/acsanm.7b00139.

[31] L. Wang, M. Li, B. Li, M. Wang, H. Zhao, F. Zhao, Electrochemical sensor based on laser-induced graphene for carbendazim detection in water, Foods 12 (2023) 2277, https://doi.org/10.3390/foods12122277.

[32] S. Baachaoui, W. Mabrouk, K. Charradi, B. Slimi, A.M. Ramadan, R.M.I. Elsamra, A. Alhussein, S.M.A.S. Keshk, N. Raouafi, Laser-induced porous graphene electrodes from polyketimine membranes for paracetamol sensing, R. Soc. Open Sci. 10 (2023) 230294, https://doi.org/10.1098/rsos.230294.

[33] B. Ouedraogo, S. Baachaoui, A. Tall, I. Tapsoba, N. Raouafi, Laser-induced graphene electrodes on polyimide membranes modified with gold nanoparticles for the simultaneous detection of dopamine and uric acid in human serum, Microchim. Acta 190 (2023) 316, https://doi.org/10.1007/s00604-023-05909-6.

[35] B. Mekassa, P.G.L. Baker, B.S. Chandravanshi, M. Tessema, Synthesis, characterization, and preparation of nickel nanoparticles decorated electrochemically reduced graphene oxide modified electrode for electrochemical sensing of diclofenac, J. Solid State Electrochem. 22 (2018) 3607–3619, https://doi.org/10.1007/s10008-018-4071-3.

[36] D.T.N. Hoa, N.T.T. Tu, L.V.T. Son, L.V.T. Son, T.T.T. Toan, P.L.M. Thong, D. N. Nhiem, P.K. Lieu, D.Q. Khieu, Electrochemical determination of diclofenac by using ZIF-67/g-C_3N_4 modified electrode, Adsorpt. Sci. Technol. 2021 (2021) e7896286, https://doi.org/10.1155/2021/7896286.

[37] G. Zhang, J. Zhang, M. Zhang, X. Wang, Polycondensation of thiourea into carbon nitride semiconductors as visible light photocatalysts, J. Mater. Chem. 22 (2012) 8083–8091, https://doi.org/10.1039/C2JM00097K.

[38] O. Salah, F.K. Algethami, W. Mabrouk, S. Baachaoui, F.M. Abdel-Haleem, T. Ben Nasr, N. Raouafi, Laser-engineered graphene electrodes on aminated

polyethersulfone/carbon black membranes for electrochemical analysis, ChemPlusChem 90 (2025) e202500262.
[39] A. Rabti, S. Baachaoui, O. Ghodbane, N. Raouafi, Laser-ablated graphene electrodes modified with redox melanin-like film for redox capacitive sensing via the scavenging of nitrite ions, Food Chem. 469 (2025) 142509, https://doi.org/10.1016/j.foodchem.2024.142509.
[40] I. Diédhiou, A. Sebei, M. Fall, S.B. Aoun, R. Zarrougui, N. Raouafi, Simultaneous detection of trace Pb(II) and Cd(II) cations in ore samples by anodic stripping analysis using pMO/erGO-modified glassy carbon electrodes, Electroanalysis 35 (2023) e202300072, https://doi.org/10.1002/elan.202300072.
[41] R.S. Nicholson, Theory and application of cyclic voltammetry for measurement of electrode reaction kinetics, Anal. Chem. 37 (1965) 1351–1355, https://doi.org/10.1021/ac60230a016.
[42] H. Matsuda, Y. Ayabe, Zur Theorie der Randles-Sevčikschen Kathodenstrahl-Polarographie, Zeitschrift für Elektrochemie, Berichte der Bunsengesellschaft für physikalische Chemie 59 (1955) 494–503, https://doi.org/10.1002/bbpc.19550590605.
[43] F. Tuinstra, J.L. Koenig, Raman spectrum of graphite, J. Chem. Phys. 53 (1970) 1126–1130, https://doi.org/10.1063/1.1674108.
[44] L.G. Cançado, et al., General equation for the determination of the crystallite size La of nanographite by Raman spectroscopy, Appl. Phys. Lett. 88 (2006) 163106, https://doi.org/10.1063/1.2196057.
[45] R. Ye, D.K. James, J.M. Tour, Laser-induced graphene: from discovery to translation, Adv. Mater. 31 (2019) 1803621, https://doi.org/10.1002/adma.201803621.
[46] P.V. Zinin, L.-C. Ming, S.K. Sharma, V.N. Khabashesku, X. Liu, S. Hong, S. Endo, T. Acosta, Ultraviolet and near-infrared Raman spectroscopy of graphitic C3N4 phase, Chem. Phys. Lett. 472 (2009) 69–73, https://doi.org/10.1016/j.cplett.2009.02.068.
[47] Z. Masood, H. Muhammad, I.A. Tahiri, Comparison of different electrochemical methodologies for electrode reactions: a case study of paracetamol, Electrochem 5 (2024) 57–69, https://doi.org/10.3390/electrochem5010004.
[48] K. Griffiths, C. Dale, J. Hedley, M.D. Kowal, R.B. Kaner, N. Keegan, Laser-scribed graphene presents an opportunity to print a new generation of disposable electrochemical sensors, Nanoscale 6 (2014) 13613–13622, https://doi.org/10.1039/C4NR04221B.
[49] T.A. Silva, H. Zanin, PaulW May, E.J. Corat, O. Fatibello-Filho, Electrochemical performance of porous diamond-like carbon electrodes for sensing hormones, neurotransmitters, and endocrine disruptors, ACS Appl. Mater. Interfaces 6 (2014) 21086–21092, https://doi.org/10.1021/am505928j.
[50] C. Bosch-Navarro, Z.P.L. Laker, J.P. Rourke, N.R. Wilson, Reproducible, stable and fast electrochemical activity from easy to make graphene on copper electrodes, Phys. Chem. Chem. Phys. 17 (2015) 29628–29636, https://doi.org/10.1039/C5CP04070A.
[51] M.S. Kavai, L.F. de Lima, W.R. de Araujo, A disposable and low-cost laser-scribed graphene electrochemical sensor for simultaneous detection of hydroquinone, paracetamol and methylparaben, Mater. Lett. 330 (2023) 133211, https://doi.org/10.1016/j.matlet.2022.133211.
[52] K. Kimuam, N. Rodthongkum, N. Ngamrojanavanich, O. Chailapakul, N. Ruecha, Single step preparation of platinum nanoflowers/reduced graphene oxide electrode as a novel platform for diclofenac sensor, Microchem. J. 155 (2020) 104744, https://doi.org/10.1016/j.microc.2020.104744.
[53] A. Afkhami, A. Bahiraei, T. Madrakian, Gold nanoparticle/multi-walled carbon nanotube modified glassy carbon electrode as a sensitive voltammetric sensor for the determination of diclofenac sodium, Mater. Sci. Eng. C 59 (2016) 168–176, https://doi.org/10.1016/j.msec.2015.09.097.
[54] T. Kokab, A. Shah, M.A. Khan, M. Arshad, J. Nisar, M.N. Ashiq, M.A. Zia, Simultaneous femtomolar detection of paracetamol, diclofenac, and orphenadrine using a carbon nanotube/zinc oxide nanoparticle-based electrochemical sensor, ACS Appl. Nano Mater. 4 (2021) 4699–4712, https://doi.org/10.1021/acsanm.1c00310.
[55] G. Sridharan, S. Balu, R. Atchudan, C. Govindasamy, D. Ganapathy, S. Arya, A. K. Sundramoorthy, Electrochemical detection of diclofenac and clindamycin using ZnO nanorods/RGO nanocomposite modified electrode, RSC Adv. 15 (2025) 49094–49108, https://doi.org/10.1039/D5RA07011B.
[56] M.M. El-Wekil, S.A. Alkahtani, H.R.H. Ali, A.M. Mahmoud, Advanced sensing nanomaterials based carbon paste electrode for simultaneous electrochemical measurement of esomeprazole and diclofenac sodium in human serum and urine samples, J. Mol. Liq. 262 (2018) 495–503, https://doi.org/10.1016/j.molliq.2018.04.120.
[57] K. Torrarit, Y. Thipwimonmas, S. Cotchim, S. Kongkeaw, A. Phonchai, W. Limbut, An electrochemical diclofenac sensor based on an electrode modified with nitrogen-doped biomass-derived carbon and molybdenum trioxide nanoparticles, Talanta 298 (2026) 128936, https://doi.org/10.1016/j.talanta.2025.128936.
[58] M. Zamani, V. Yang, L. Maziashvili, G. Fan, C.M. Klapperich, A.L. Furst, Surface requirements for optimal biosensing with disposable gold electrodes, ACS Meas. Sci. Au 2 (2022) 91–95, https://doi.org/10.1021/acsmeasuresciau.1c00042.